Thermodynamic properties of paracetamol impurities 4-nitrophenol and 4'-chloroacetanilide and the impact of such impurities on the crystallisation of paracetamol from solution

René R.E. Steendam, Leila Keshavarz, Brian P. de Souza, PATRICK J FRAWLEY

The Journal of Chemical Thermodynamics
2019 133, pp. 85-92

Thermodynamic properties of Paracetamol Impurities 4-nitrophenol and 4'-chloroacetanilide and the impact of such Impurities on the Crystallisation of Paracetamol from solution

René R.E. Steendam Leila Keshavarz Brian de Souza Patrick J. Frawley

https://doi.org/10.1016/j.jct.2019.02.004

Thermodynamic properties of Paracetamol Impurities 4-nitrophenol and 4'-chloroacetanilide and the impact of such Impurities on the Crystallisation of Paracetamol from solution

René R. E. Steendam[†*], Leila Keshavarz[†], Brian de Souza and Patrick J. Frawley

School of Engineering, Synthesis and Solid State Pharmaceutical Centre (SSPC), Bernal Institute, University of Limerick, Castletroy, Co. Limerick, Ireland

† Equal contribution

* Corresponding author. Tel: +353852765494

E-mail: renesteendam@gmail.com

ABSTRACT[1]

The impact of structurally-related additives and impurities on active pharmaceutical ingredients is an essential yet poorly understood area. This work describes the characterisation of temperature-dependent solid-liquid properties of 4-nitrophenol and 4'chloroacetanilide in four different alcohols and their effect as impurities on the crystallisation of paracetamol. The solubility of 4-nitrophenol appeared to be significantly higher than paracetamol whereas the solubility of 4'chloroacetanilide was lower than paracetamol. The solubility difference between the impurities could be rationalised based on their molecular structure and hydrogen bonding interactions. The solubility data was modelled using empirical and thermodynamic models. Recrystallisation of paracetamol from solution containing the highly soluble 4-nitrophenol impurity resulted in small uniformly sized high purity paracetamol crystals whereas the presence of the poorly soluble

[1] *Abbreviations:* CA, 4'-chloroacetanilide; DSC, differential scanning calorimetry; GC, gas chromatography; HPLC, high performance liquid chromatography; LC, liquid chromatography; MSE, mean squared error; MW, molecular weight; NP, 4-nitrophenol; PA, paracetamol; PTFE, polytetrafluoroethylene; RMSE, root mean square error; SEM, scanning electron microscopy; UV, ultraviolet; XRPD, x-ray powder diffraction.

4’chloroacetanilide impurity induced the formation of large needle shaped crystals of paracetamol. These differences in crystallisation are a consequence of the solubility difference and the different functional groups of paracetamol and its impurities. Overall this study serves as fundamental information for the development of crystallisation approaches for the purification of paracetamol from its main impurities.

KEYWORDS

Crystallisation, solubility, impurity, additive, morphology, thermodynamic modelling

1. INTRODUCTION

Reactive disubstituted aromatic compounds are frequently used in the manufacture of pharmaceuticals to enable the synthetic steps that lead to the desired product. However, the reactive nature of such intermediates also leads to the formation of organic impurities that are structurally similar to the target compound. This is for example reflected in the synthesis of paracetamol which mainly yields paracetamol together with trace amounts of unwanted 1,4-disubstituted aromatic impurities. Two of the main impurities in the manufacture of paracetamol (PA) are 4-nitrophenol (NP) and 4’-chloroacetanilide (CA) (Figure 1).[1]

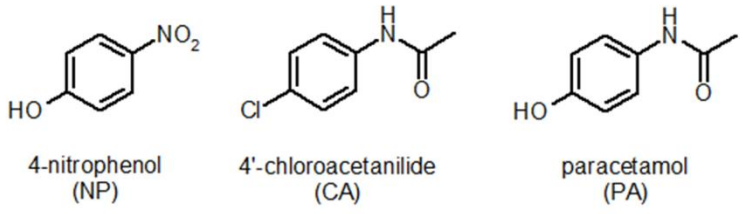

Fig. 1. The chemical structures of paracetamol and two of its main impurities.

PA is known to be able to crystallise as three monotropic polymorphs. At room temperature, monoclinic Form I[2] is the most stable form, followed by metastable orthorhombic Form II[3] and the highly unstable Form III.[4] 4-Aminophenol is the starting material in the final step of the synthesis of PA and is obtained through reduction of NP. NP can crystallise as two polymorphic

forms of which the β-form (β-NP) could undergo an irreversible transformation into the light unstable α-form (α-NP) at temperatures between (331 and 366 K).[5, 6] CA is structurally the same as PA except that CA has a chlorine atom instead of an alcohol group at the 4-position. Only one crystalline form has been reported for CA.[7]

The level of impurities in pharmaceutical products should strictly be kept below a specified amount in order to guarantee the desired biological effect of the pharmaceutical and to avoid undesired side effects such as a change in polymorphism or chirality of the product.[8-10] An efficient purification technique to remove impurities is solvent crystallisation as the crystalline lattice of the target compound is typically able to selectively incorporate target molecules in preference over impurities.[11] Important process parameters in solvent crystallisation, including the metastable zone width and nucleation rates, rely on the solubility of the compound. Thermodynamic calculations based on solubility data of impurities and the effect of impurities on the solubility of the target compound is therefore essential for the design and use of solvent crystallisation. The presence of ionic impurities generally leads to an increase in the solubility of inorganic salts.[12, 13] However, the effect of organic impurities on the solubility of pharmaceuticals is more complex and less understood. PA is one of the most widely used model systems in crystallisation research yet the effect of its main impurities on the solid-liquid properties of PA remain unreported. Solid-liquid measurements for PA impurities might prove challenging as these compounds are reported to form different polymorphs and are prone to undergo oxidation and decomposition. The solubility of NP in water [14, 15] and ethanol [16] is reported but it is unclear which polymorph was used in those studies. Except for the solubility of NP in water and ethanol, no solid-liquid data is currently reported for NP or CA to the best of our knowledge. Moreover, it is unclear if the polymorphism of the impurities is affected by solution crystallisation and whether impurities influence the solid-liquid properties of PA.

This work describes the solubility of two of the main impurities of PA and their effect on the crystallization of PA. First a polymorphic screening was carried out to determine the polymorphic nature of the solids used in this study. In addition, solution phase analysis was conducted to determine the stability of the impurities in solution. Secondly, equilibrium solubility measurements are reported for α-NP and CA in four different alcohols (ethanol, 2-propanol, 1-pentanol and 1-butanol) over the

temperature range (278.15 to 318.15) K. In previous solubility measurements of pure PA the same solvents were used and were therefore chosen in the present study for comparison.[17] The solubility data was analysed using empirical and thermodynamic models. Finally the effect of the impurities on the crystal morphology and purity of PA from solution crystallisation experiments are described.

The results reported herein represent fundamental information for the design of solvent crystallisation strategies that can be used for the purification of PA from its main impurities.

2. THERMODYNAMIC MODELLING

The solubility of the impurities NP and CA and the solubility of PA in the presence of NP and CA in the selected solvents as a function of temperature are correlated with the empirical modified Apelblat equation, which is defined as

$$\ln(x_2) = a_{\mathrm{A}} + \frac{b_{\mathrm{A}}}{T} + c_{\mathrm{A}} \ln(T) \quad (1)$$

where x_2 is the solute molar fraction at temperature T in Kelvin and a_{A}, b_{A} and c_{A} are the three adjustable parameters which can be obtained through regression.[18]

The Margules, Van Laar, Wilson and NRTL models are used to describe the solubility of the pure compounds NP and CA. These activity coefficient models account for deviations from ideal solution behaviour and use a solid-liquid equilibrium equation

$$\ln(x_2\gamma_2) = \frac{\Delta H_{\mathrm{fus}}}{R}\left(\frac{1}{T_{\mathrm{t}}} - \frac{1}{T}\right) - \frac{\Delta C_{\mathrm{P}}}{R}\left(\frac{1}{T_{\mathrm{t}}} - \frac{1}{T}\right) - \frac{\Delta C_{\mathrm{P}}}{R}\ln\left(\frac{T_{\mathrm{t}}}{T}\right) \quad (2)$$

where γ_2 is the activity coefficient, ΔH_{fus} the fusion enthalpy of the solute, T_{t} the triple-point temperature, ΔC_{P} the difference of the heat capacity of a solute between the liquid- and solid state and R is the universal gas constant (8.314 $\mathrm{J{\cdot}K^{-1}{\cdot}mol^{-1}}$).[18] Due to the small value of ΔC_{P} with respect to the first term on the right side of equation, ΔC_{P} can be neglected.[18] The triple-point temperature T_{t}

is nearly equal to the melting temperature T_m of the compound and therefore equation 2 can be simplified to

$$\ln(x_2) = \frac{\Delta H_{\text{fus}}}{R}\left(\frac{1}{T_m} - \frac{1}{T}\right) - \ln(\gamma_2) \quad (3)$$

The experimental activity coefficients γ_2 can be calculated by inserting the experimental solubility values x_2 measured at temperature T, the enthalpy of fusion ΔH_{fus} and the melting temperature T_m into equation 3. The ideal solubility can be calculated by setting γ_2 =1.

The experimental activity coefficients γ_2 were correlated to the Margules, van Laar, Wilson and NRTL models. The Margules model considers the temperature dependence explicitly and is expressed as

$$\ln(\gamma_2) = \frac{A}{RT}(1 - x_2)^2 \quad (4)$$

where A is an adjustable parameter.

In the van Laar equation, the temperature dependence is implicit and the van Laar equation can be written as

$$\ln(\gamma_2) = \frac{B_{vl}}{\left(1+\frac{B_{vl}x_2}{A_{vl}x_1}\right)^2} \quad (5)$$

where A_{vl} and B_{vl} are the adjustable van Laar parameters and x_i is the mole fraction of component i.

The Wilson model can be expressed as

$$\ln(\gamma_2) = -x_2\left(\frac{\Lambda_{12}}{x_1+\Lambda_{12}x_2} - \frac{\Lambda_{21}}{x_2+\Lambda_{21}x_1}\right) - \ln(x_2 + \Lambda_{21}x_1) \quad (6)$$

in which

$$\Lambda_{ij} = \frac{v_j}{v_i} \exp\left(-\frac{\lambda_{ij}}{RT}\right) \text{ with } i \neq j \text{ and } i,j = 1,2 \quad (7)$$

and where v_i is the molar volume of the solute and v_j that of the solvent. Λ_{ij} are the cross-interaction energy parameters ($J \cdot mol^{-1}$) between the components *i* and *j*.

The NRTL model considers that the local concentration around a molecule is different from the concentration in the bulk. The NRTL equation is expressed as

$$\ln(\gamma_2) = x_1^2 \left[\left(\tau_{12} \frac{G_{12}}{x_2 + x_1 G_{12}}\right)^2 + \frac{\tau_{21} G_{21}}{(x_1 + x_2 G_{21})^2}\right] \quad (8)$$

in which

$$G_{ij} = \exp(-\alpha \tau_{ij}) \text{ with } i \neq j \text{ and } i,j = 1,2 \quad (9)$$

and

$$\tau_{ij} = \frac{g_{ij}}{RT} \text{ with } i \neq j \text{ and } i,j = 1,2 \quad (10)$$

where g_{ij} ($J \cdot mol^{-1}$) are the model parameters which relate to the cross-interaction energy and where α is the parameters that account for the non-randomness of the solution.

The parameters of each activity coefficient model were estimated by using the nonlinear least-squares algorithm *nlinfit* in Matlab to solve

$$\min_{\theta \in \mathcal{R}} \sum_{i=1}^{N} \left[\ln(\gamma_{2,i})|_{\text{mod}}(T,\theta) - \ln(\gamma_{2,i})|_{\exp}(T)\right]^2 \quad (11)$$

where θ represents the parameters to be estimated for each model, each compound and each solvent used, N refers to the number of data points and where $y_{2,i|mod}$ and $y_{2,i|exp}$ refer to the model and experimental activity coefficients respectively. The activity coefficients γ_2 described in the results are the experimental activity coefficients.

Conversion from solute molar fraction x_2 to mass-fraction solubility C was carried out through

$$C = \frac{1000 x_2 MwSolute}{((1-x_2)MwSolvent + x_2 MwSolute)} \quad (12)$$

3. EXPERIMENTAL SECTION

3.1 Chemicals

The chemicals used in this study, together with their suppliers, mass fraction purity and method for purity determination are summarised in Table 1. All the chemicals were used as received without further purification. The methods employed by the supplier for the determination of the purity of PA include infrared absorption, ultraviolet absorption, thin-layer chromatography, melting point, titration and residue on ignition tests. Using our HPLC measurements, it was established that no detectable amounts of 4-aminophenol, NP or CA were present in the supplied PA.

Table 1. The sources and mass fraction purity of the materials used in this study.

Chemical Name	CAS Registry Number	Source	Mole Fraction Purity	Analysis Method
paracetamol (PA)	103-90-2	Sigma-Aldrich	0.98-1.02	several, see main text
4'-chloroacetanilide (CA)	539-03-7	Sigma-Aldrich	0.97	GC[a]
4-nitrophenol (NP)	100-02-7	Alfa Aesar	0.99	GC

deionised water	7732-18-5	distilled	-	none
ethanol	64-17-5	Honeywell	≥0.99	GC
methanol	67-56-1	Sigma-Aldrich	≥0.99	GC
2-propanol	67-63-0	Sigma-Aldrich	≥0.99	GC
1-pentanol	71-41-0	Sigma-Aldrich	≥0.99	GC
1-butanol	71-36-3	Sigma-Aldrich	≥0.99	GC
Na_2HPO_4 dibasic solution	7558-79-4	Sigma-Aldrich	≥0.99	Titration
phosphoric acid	7664-38-2	Sigma-Aldrich	≥0.85	Titration

[a]Gas Chromatography

3.2 Thermal Analysis

The melting temperature T_m and the enthalpy of fusion ΔH_f of CA were determined using a PerkinElmer Pyris-Diamond differential scanning calorimetry (DSC) instrument. The instrument was pre-calibrated by using the onset temperature for indium. A precisely weighted DSC sample of CA was inserted into the DSC and heated from (298.15 K to 468.15 K) at a rate of 10 K /min under a nitrogen flow. Standard uncertainties of the experiments were evaluated to be 0.5 K for temperature and 400 $J \cdot mol^{-1}$ for the enthalpy of melting. The onset temperature of melting, which was obtained by taking the inflection point of the DSC curve, was used as the melting temperature T_m as per the recommendation from Gesellschaft für Thermische Analyse (GEFTA) and the International Confederation for Thermal Analysis and Calorimetry (ICTAC).

3.3 Solid State Characterisation

XRPD measurements were conducted to establish the polymorphic nature of the chemicals. Crystal samples were lightly ground into a fine powder and measured on a PANalytical EMPYREAN diffractometer using Bragg−Brentano geometry and an incident beam of Cu K-Alpha radiation (λ = 1.5406 Å). Scans were performed at room temperature on a spinning silicon sample holder with a step size of 0.013° 2θ and a step time of 68 s.

To establish which polymorph of each compound was present in our solubility experiments, XRPD analysis was carried out of the solid phase samples taken from the equilibrium solubility measurements. After equilibration for 24 h at a fixed temperature, about 5 mL of the suspension was subjected to vacuum filtration. The residual crystals were completely dried at the same temperature and were measured using XRPD. The experimental XRPD patterns were compared with reference XRPD patterns which were obtained using Mercury software by converting single crystal data taken from the Cambridge Structural Database (CSD).

3.4 HPLC Analysis

The HPLC method for determining the purity of PA reported in literature has been adapted to our work.[19] An Agilent 1260 Infinity Quaternary LC was used in combination with a ZORBAX eclipse XDB-C18 column (4.6x150 mm, 3.5µ). A 0.01 M sodium phosphate buffer was prepared through the dilution of a 0.5 M phosphate buffer using deionised water (18.2 Ω) after which the buffer was brought to pH=3 using phosphoric acid. The 0.01M sodium phosphate buffer was used in combination with methanol as the mobile phase. The flowrate was set to 1.000 mL/min, the column temperature to 20 °C and the injection volume used was 5 µL. 2 mL Amber borosilicate glass vials were used for the HPLC samples. A stock solution was prepared for each compound which was subsequently diluted into a concentration range C_R. Triplicate measurements were carried out for each sample and the resulting low relative standard deviation of <1% indicated that the HPLC method was sufficiently accurate. The peak heights measured over the entire concentration range fell well below the ultraviolet (UV) detection limit of the HPLC and the absorption peaks of the different compounds did not overlap. The peak area, which was averaged over three measurements of the same sample, was plotted against 10 different concentrations and resulted in a linear calibration curve ($R^2 > 0.999$) for each compound, as shown in the Supporting Information (Figure S2).

The solute was dissolved in methanol and the resulting solution was diluted until the concentration was within the concentration range C_R of the calibration series. The ratio of PA to impurities and from that, the actual concentration of PA in the solute, was calculated from the acquired peak areas in conjunction with the calibration curves. The concentration range C_R of the

calibration series, composition of the mobile phase X, the wavelength λ of detection and the retention times t_R for each compound are summarised in the supporting information (Table S1).

3.5 Solubility Determination

The solubility of CA and NP in different solvents (ethanol, 2-propanol, 1-butanol and 1-pentanol) at 8 different temperatures (278.15 to 318.15 K, with steps of 5 K) was determined using equilibrium gravimetric solubility measurements. For a single solubility data point, one of the tested solvents was added to a glass vial containing an excess of solids of either CA or NP. The gravimetric method has been used and validated by us in previous works and the same protocol was used in the current work.[17, 20]

As per the NIST guidelines, the standard uncertainties $u(C)$ and $u(x_2)$ were determined by estimating the standard deviation of the three samples of each solubility data point. For each data point, the relative standard uncertainties $u_r(C)$ and $u_r(x_2)$ were calculated by dividing the standard uncertainties over the average solubility. The herein reported relative standard uncertainties for a specific compound were obtained by taking an average of the relative standard uncertainties of all data points for that specific compound.

4 RESULTS & DISCUSSION

In this work, a polymorphic screening is first described that shows which polymorph of each compound is used in this study. Next the solubility data of NP and CA as a function of temperature in different solvents is described which in the following section is modelled. In the final section the influence of NP and CA as impurities on crystallisation of PA is described.

4.1 Polymorphic Screening

XRPD studies were conducted to establish the polymorphic nature of PA, NP and CA used in this study. The XRPD patterns were compared with the known polymorphic forms in literature (Supporting Information S4-S6) and the results are summarised in Table 2.

Table 2. The Polymorphic Form of Each Compound Determined from Samples Obtained from the Supplier and Experiments.

Compound	Obtained From	Polymorphic Form
PA	Literature[2]	I
PA (Starting Material)	Sigma Aldrich	I
PA + 0.10 mole fraction of CA	Experiments	I
PA + 0.10 mole fraction of NP	Experiments	I
CA	Literature[7]	CA[a]
CA (Starting Material)	Sigma Aldrich	CA
CA	Experiments	CA
NP	Literature[5]	β-NP
NP	Literature[21]	α-NP
NP (Starting Material)	Alfa Aesar	α-NP
NP	Experiments	α-NP

[a]No polymorphic forms of CA are reported in literature or were found in this study.

PA was obtained as Form I from the supplier and remained stable in our solubility experiments. The crystalline form of CA obtained from the supplier was the same as the one reported in literature.[7] Although two forms are reported for NP, only α-NP was present in the starting material. It is reported in literature that a polymorphic transformation from α-NP to β-NP is not possible.[6] Indeed, in our experiments no such polymorphic transformation was observed across the full temperature range and solvents studied. During the experiments we did however observe a small colour change of α-NP crystals from yellow to red which reportedly results in insignificant changes in crystal structure and molecular dynamics.[6] Figure S6 in the supporting information shows similar XRPD patterns of α-NP crystals before and after being exposed to visible light for 48 h.

4.2 Solid-Liquid Equilibria of CA and α-NP

The mass-fraction solubility *C* of CA and α-NP as a function of temperature *T* in all four tested solvents is tabulated in the Supporting Information (Table S2 and S3 respectively) and plotted in Figure 2. The solubility of each compound was found to increase with increasing temperature in all four tested alcohols. Solution studies of both compounds involving HPLC measurements across the full temperature range and solvent range showed no signs of degradation of the compounds.

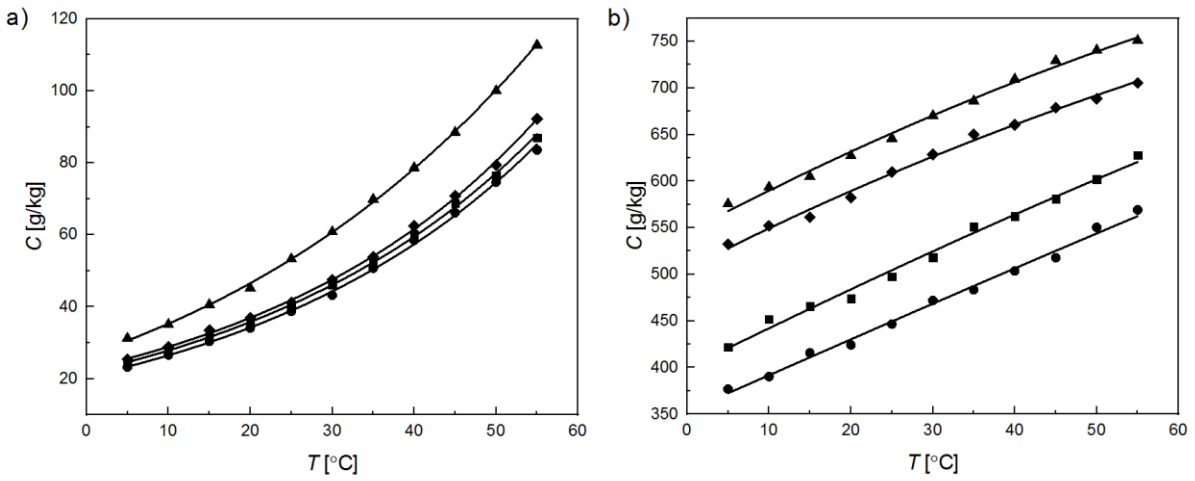

Fig. 2. The mass-fraction solubility (*C*) versus temperature (*T*) in ▲, ethanol; ♦, 2-propanol; ■, 1-butanol; ●, 1-pentanol for: (a) CA; (b) α-NP. The data is fitted using the NRTL model.

The experimentally determined mass-fraction solubility of NP in ethanol was compared with literature values (Figure 3). The data show that the mass-fraction solubility is similar within the temperature range (20-45) °C. The variations in mass-fraction solubility outside the temperature range (20-45) °C might be explained by the difference in methodology for solubility determination. In the literature report, solubility was measured by monitoring the disappearance of crystals whereas our approach involved isothermal equilibrium measurements. In addition, the literature report does not mention which polymorph of NP was used and the variations in mass-fraction solubility might be the result of measurements on different polymorphs.

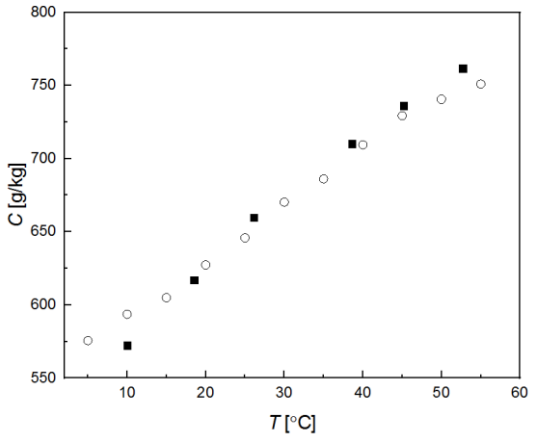

Fig. 3. The mass-fraction solubility (*C*) versus temperature (*T*) for NP in ethanol: ○ this work obtained through isothermal equilibrium gravimetric analysis; ■ Carrick obtained through a variation of the synthetic method [16].

The mass-fraction solubility of both CA and α-NP across the full temperature range follows the order ethanol > 2-propanol > 1-butanol > 1-pentanol. The solubility decreases monotonically with increasing number *n* of carbon atoms in the alkyl chain of the solvent (Figure 4). Solvents with longer alkyl chain lengths exhibit lower polarity and have more difficulty forming hydrogen bonds with the solute, overall leading to a lower solubility. The mass-fraction solubility of α-NP increases almost linearly whereas the mass-fraction solubility of CA increases exponentially with increasing number *n* of carbon atoms in the alkyl chain of the solvent. This solubility relationship for CA was also found for PA[22] which is very similar to CA in terms of molecular structure. The relative high solubility of α-NP could be attributed to its nitro group which, like the alcohol group, forms hydrogen bonds with the solvent molecules. Moreover, the electron withdrawing nature of the nitro group is expected to enhance the hydrogen-donating capability of the alcohol group which could further enhance hydrogen bonding and with that the solubility of NP in alcohols.

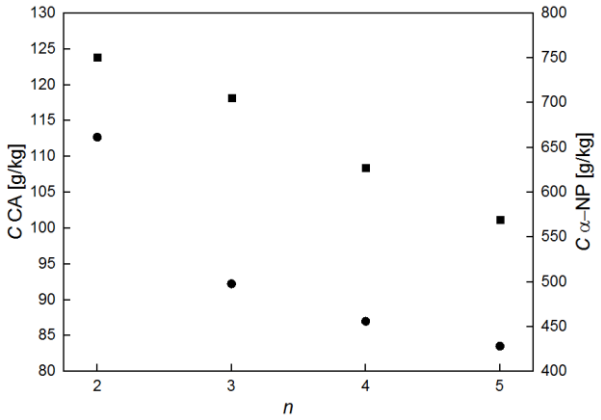

Fig. 4. The mass-fraction solubility (C) of ●, CA and ■, α-NP versus the number n of carbon atoms in the alkyl chain of the solvent at temperature T=55 °C.

4.3 Thermodynamic Modelling of CA and α-NP

For the description of the solubility of CA and α-NP using the thermodynamic models, experimental activity coefficients γ_2 were needed which were calculated using the melting temperature T_m and the enthalpy of fusion ΔH_{fus}. The melting temperature T_m and the enthalpy of fusion ΔH_{fus} of α-NP is 381 K and 12 kJ mol^{-1} respectively.[6] Through DSC measurements we found that the melting temperature T_m of CA, determined as the onset of melting, is 448.80 K. This value corresponds to some of the reported literature values [23, 24], although most of the published melting temperatures T_m of CA fall within the temperature range of (451.15-452.15) K[25-29]. The reported melting temperature range might have been determined from peak temperatures, as in our analysis the peak temperature would result in 451.88 K. For the estimation of experimental activity coefficients γ_2 we used the onset of melting of 448.80 K.

The enthalpy of fusion ΔH_{fus} of CA reported in literature corresponds to 40.75 kJ·mol^{-1} which was measured through the depression of the freezing point of the amine by benzene, dibromobenzene, or benzil in a Beckmann apparatus.[30] In our experiments, we used DSC to obtain an enthalpy of fusion ΔH_{fus} of CA of 27.14 kJ·mol^{-1}, which is similar to the enthalpy of fusion of 27.6 kJ·mol^{-1} of the structurally-related PA.[31] The difference between our experimental value and the literature value may be due to the difference in measurement technique.

Plots of the natural logarithm of the experimental activity coefficients γ_2 for CA and α-NP as a function of temperature T are shown in Figure 5a. From eq 2 it follows that the experimental activity coefficient γ_2 is inversely proportional to the solute mole fraction x_2. This is reflected in the obtained solute mole fraction x_2 (Table S2 and S3), which shows an inverse relationship to the activity coefficients γ_2. The slightly larger deviation of CA from ideal solubility ($\ln(\gamma_2) = 0$) could be explained by its more complex chemical structure as compared to NP. The activity coefficients γ_2 exhibit a trend in relation to solvent type. The order of activity coefficients γ_2 as a function of solvent can be explained by the chain length of the solvent, with short-chain alcohols resulting in stronger hydrogen bonding which result in larger deviations from ideal solubility. The activity coefficients γ_2 for pure PA range from (0.2 to 0.8) [17] and are therefore similar to the activity coefficients γ_2 of CA. This could be explained by the similarities in terms of molecular structure.

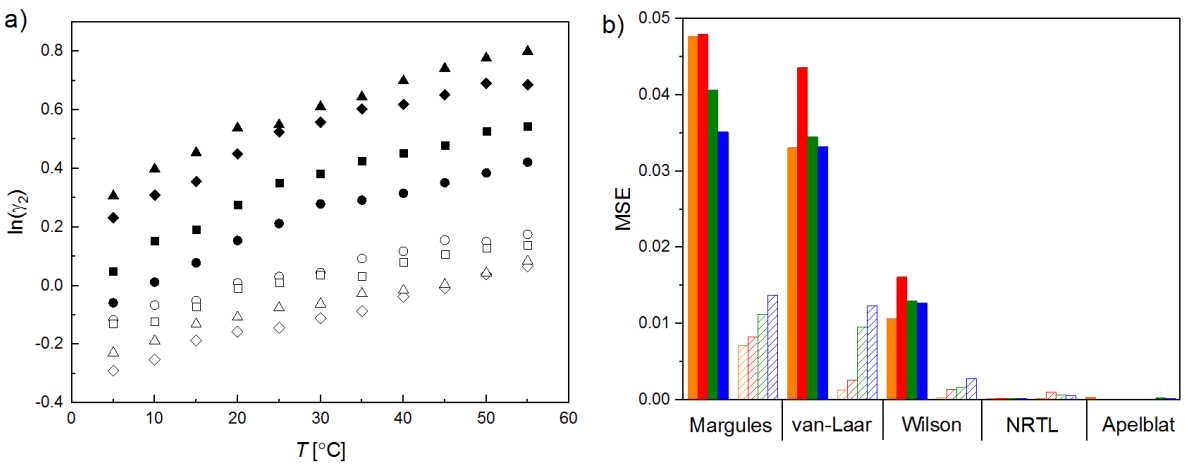

Fig. 5. a) Logarithm of the experimental activity coefficients (γ_2) versus temperature (T) for CA (filled symbols) and α-NP (open symbols) in ▲, ethanol; ♦, 2-propanol, ■, 1-butanol and ●, 1-pentanol. b) The quality of fit expressed as the mean square error (MSE) for CA (filled) and α-NP (shaded) for each model. From left to right, the bars represent ethanol (orange), 2-propanol (red), 1-butanol (green) and 1-pentanol (blue).

The calculated activity coefficients were used to model the experimental solubility data using four activity coefficient models. The estimated binary coefficients of each thermodynamic model and

the Apelblat parameters are reported in the Supporting Information (Table S4-S6). The quality of fit of these models to the experimental data is expressed as the mean square error (MSE) which is tabulated in the Supporting Information (Table S4 and S7) and plotted in Figure 5b. For each compound, the quality of fit of the model to the experimental data increases in the order Margules < van-Laar < Wilson < NRTL < Apelblat. This order can be explained by the number of adjustable parameters used in each of the models where more adjustable parameters lead to a better fit. The number of adjustable parameters is the same for the van-Laar model and the Wilson model, yet the temperature dependency is implicit in the van-Laar model which results in a poorer fit as compared to the Wilson model in which the temperature dependence is explicit. Except for ethanol, the quality of fit for CA increases with increasing solubility. For α-NP the quality of fit of the Margules, van-Laar and Wilson model increases with decreasing solubility. For the other models, no apparent trend was observed.

4.4 Comparison of CA and α-NP to Paracetamol

Figure 6 shows the difference in mass-fraction solubility ΔC (C impurity – C paracetamol) between α-NP and PA (positive values) and CA and PA (negative values) as a function of temperature T in each of the alcohols. An increase in the difference in mass-fraction solubility between impurity and PA (i.e. a larger deviation from 0 in Figure 6) is expected to lead to an increase in the efficiency of separation of the impurity from PA through crystallisation.

The mass-fraction solubility of CA is lower than that of PA and the difference increases in the order 1-pentanol < 1-butanol < 2-propanol < ethanol. Furthermore, the mass-fraction solubility difference increases with increasing temperature in all solvents tested. The most efficient separation conditions to remove CA from PA are expected to involve high temperatures and short chain alcohols (i.e. ethanol). The relative low mass-fraction solubility of CA could be ascribed to its lack of having an alcohol group which in PA notably enhances the solubility due to its hydrogen bond donating capability.

The mass-fraction solubility C of α-NP is significantly larger than the mass-fraction solubility of PA in all tested solvents. Such large differences in solubility suggest that separation of α-NP from

PA should be efficient. The difference in mass-fraction solubility between NP and PA increases in the order 1-pentanol < 1-butanol < ethanol < 2-propanol. Therefore, the most suitable solvent to remove α-NP from PA would be 2-propanol.

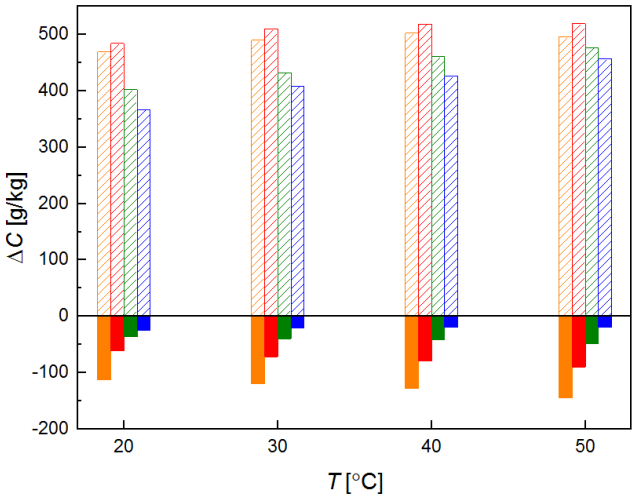

Fig. 6. a) The mass-fraction solubility difference Δ*C* between the mass-fraction solubility of α-NP and PA (positive values) and CA and PA (negative values) as a function of temperature (*T*). Mass-fraction solubility data of PA was used from literature.[17] From left to right, the bars represent the mass-fraction solubility difference in ethanol (orange), 2-propanol (red), 1-butanol (green) and 1-pentanol (blue).

The similarity between CA and PA in terms of molecular structure (Figure 1) is reflected in the similar solubility of each compound. On the other hand, the molecular structure of α-NP differs significantly from PA and hence its solubility is markedly different.

4.5 Crystallisation of Paracetamol in the Presence of Impurities

The effect of the impurities on the crystal shape of PA was analysed using scanning electron microscopy (SEM). In the absence of impurities, cooling crystallisation of PA at temperature *T*=15 °C from 2-propanol resulted in an apparent wide size distribution of tabular crystals (Figure 7a). Cooling crystallisation of PA from 2-propanol in the presence of 0.10 mole fraction of α-NP resulted in an apparent narrow size distribution of small tabular crystals (Figure 7b). The crystal shape of PA did not

change as a result of the α-NP impurity which suggests that the impurity did not selectively inhibit the crystal growth of a specific crystal face. On the other hand, the molecular similarity between CA and PA resulted in face specific crystal growth inhibition giving rise to needle-shaped crystals of PA (Figure 7c). These changes in crystal habit were also observed in combination with 0.001 mole fractions of impurities. Despite these dramatic changes in crystal shape, the presence of the impurities did not change the polymorphic form of PA Form I across all the solvents and temperature tested in this work (Figure S4). Therefore, although the impurities inhibit the crystal growth rate, the intermolecular interactions between molecules in PA Form I are sufficiently strong to retain its polymorphic form.

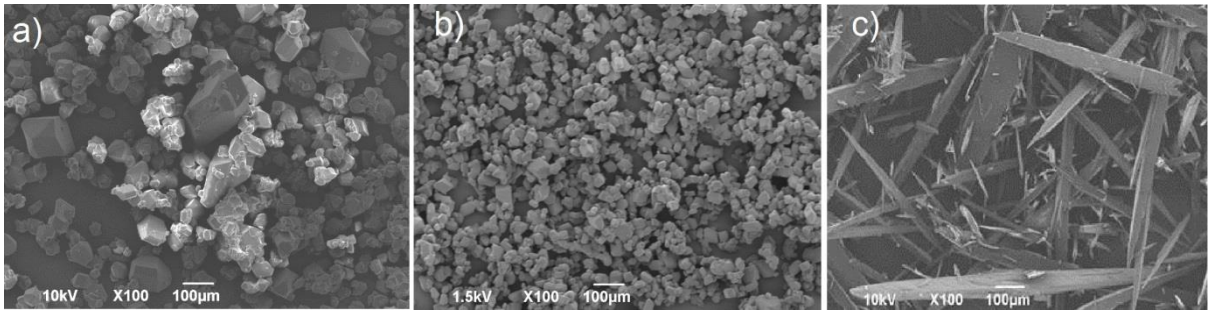

Fig. 7. SEM Images of PA obtained through cooling crystallisation from 2-propanol at temperature (*T*) of 15 °C: (a) without impurities; (b) with 0.10 mole fraction of α-NP; (c) with 0.10 mole fraction of CA.

In the presence of 0.10 mole fraction of α-NP, cooling crystallisation experiments of PA typically resulted in product crystals containing >0.99 mole fraction of PA. The significant difference in functional groups between α-NP and PA prevents incorporation of α-NP molecules into the growing PA crystal lattice. In addition, α-NP is much more soluble in alcohols than PA (Figure 6) and recrystallization of PA from α-NP therefore proceeds in a highly selective manner, giving highly pure PA products crystals. Therefore, purification of PA from α-NP proceeds efficiently as is reflected in our recent study where mother liquor fractions were recycled in crystallisation experiments.[32]

On the other hand, crystallisation experiments of PA in the presence of 0.10 mole fraction of CA resulted in product crystals with lower purities in the order of 0.98 mole fraction of PA. Due to

the structural similarity between CA and PA, CA is expected to easily incorporate into the crystal lattice of PA. In addition, CA has a similar solubility as compared to PA in alcohols and recrystallization of PA from CA was therefore found to be challenging.

5. CONCLUSIONS

The solubility of 4-nitrophenol (NP) and 4'-chloroacetanilide (CA) increases with increasing temperature and solvent order ethanol > 2-propanol > 1-butanol > 1-pentanol. The quality of fit of the tested thermodynamic models to the experimental data increases in the order Margules < van-Laar < Wilson < NRTL < Apelblat. The solubility of α-NP is significantly higher than the solubility of paracetamol (PA) whereas the solubility of CA is slightly lower than that of PA. Recrystallisation of PA in the presence of α-NP resulted in small and uniform pure PA crystals whereas recrystallisation of PA in the presence of CA resulted in large needle-shaped PA crystals contaminated with CA. These results can be rationalised by the molecular similarities and solubility differences between the impurities and the target compound. Overall this study provides fundamental information on the solid-liquid properties of structurally-related impurities of PA that are essential for the design of solution crystallisation strategies for the purification of PA from its main impurities.

ASSOCIATED CONTENT

Supporting Information

DSC Thermogram of CA (Figure S1); HPLC conditions (Table S1); HPLC calibration lines for PA, NP, and CA (Figure S2); XRPD patterns of PA (Figure S3); XRPD patterns of CA (Figure S4); XRPD patterns of CA (Figure S5); XRPD patterns of α-NP before and after being exposed to visible light (Figure S6); Solubility data CA (Table S2); Solubility data α-NP (Table S3); Apelblat parameters and MSE (Table S4); Binary coefficients for CA (Table S5); Binary coefficients for α-NP (Table S6); MSE of the fitted thermodynamic models (Table S7).

AUTHOR INFORMATION

ORCID

René R. E. Steendam: 0000-0002-3363-4160

Brian De Souza: 0000-0002-4469-7802

Funding

This research has been conducted as part of the Synthesis and Solid State Pharmaceutical Centre (SSPC) and funded by Science Foundation Ireland (SFI) under Grant 12/RC/2275.

Notes

The authors declare no competing financial interest.

NOMENCLATURE

Abbreviations

CA	4’-chloroacetanilide
DSC	differential scanning calorimetry
GC	gas chromatography
HPLC	high performance liquid chromatography
LC	liquid chromatography
MSE	mean squared error
MW	molecular weight
NP	4-nitrophenol
PA	paracetamol
PTFE	polytetrafluoroethylene
SEM	scanning electron microscopy
UV	ultraviolet
XRPD	x-ray powder diffraction

Variables and Constants with Units and Symbols

a_A	First Apelblat parameter
a_2	Solute activity
A	Margules binary interaction parameter
A_{vl}	First Van-Laar interaction parameter
b_A	Second Apelblat parameter
B_{vl}	Second Van-Laar interaction parameter
c_A	Third Apelblat parameter
C	Mass-fraction solubility [$g_{sol}/Kg_{solution}$]
C_R	Concentration range of the HPLC calibration series
ΔC_p	Exchange of heat capacity at constant pressure evaluated at melting point [J/mol/K]
g_{ij}	NRTL binary interaction parameter
G_{ij}	Corrected temperature-dependent NRTL binary interaction parameter
ΔH_{fus}	Exchange of enthalpy of fusion evaluated at melting point [KJ/mol]
I	Impurity content [mole fraction]
k	Boltzmann constant [J/K]
Mw_{solute}	Molecular weight solute [g/mol]
$Mw_{solvent}$	Molecular weight solvent [g/mol]
n	Number of carbon atoms of solvent
P	Pressure [Pa]
R	Ideal gas constant [J/mol/K]
T	Temperature [°C]
T_t	Triple-point temperature [K]
T_m	Melting temperature [K]
t_R	Retention time HPLC peaks [min]
v_i	Molar volume of the solute [cm^3/mol]
v_j	Molar volume of the solvent [cm^3/mol]
x_2	Solute molar fraction

X	Composition of HPLC mobile phase [v/v%]

Greek Letters

α	NRTL non-randomness parameter
α-NP	The alpha polymorphic form of 4-nitrophenol
β-NP	The beta polymorphic form of 4-nitrophenol
γ_2	Activity coefficient referred to the solute
λ	Wavelength used in HPLC analysis [nm]
λ_{ij}	Wilson binary interaction parameter
λ_x	Wavelength used in XRPD measurements [Å]
Λ_{ij}	Temperature-dependent Wilson binary interaction parameter
τ_{ij}	Temperature-dependent NRTL binary interaction parameter
θ	Set of binary interaction parameters for each activity equation model

REFERENCES

[1] O. Călinescu, I.A. Badea, L. Vlădescu, V. Meltzer, E. Pincu, HPLC Separation of Acetaminophen and its Impurities Using A Mixed-mode Reversed-Phase/Cation Exchange Stationary Phase, Journal of Chromatographic Science 50 (2012) 335-342.
[2] M. Haisa, S. Kashino, R. Kawai, H. Maeda, The Monoclinic Form of p-Hydroxyacetanilide, Acta Crystallogr. B 32 (1976) 1283-1285.
[3] N. Drebushchak Tatyana, V. Boldyreva Elena, Variable temperature (100–360 K) single-crystal X-ray diffraction study of the orthorhombic polymorph of paracetamol (p-hydroxyacetanilide), Zeitschrift für Kristallographie - Crystalline Materials, 2004, pp. 506.
[4] M.-A. Perrin, M.A. Neumann, H. Elmaleh, L. Zaske, Crystal structure determination of the elusive paracetamol Form III, Chemical Communications (2009) 3181-3183.
[5] P. Coppens, G.M.J. Schmidt, The crystal structure of the metastable ([beta]) modification of p-nitrophenol, Acta Crystallographica 18 (1965) 654-663.
[6] G. Wojcik, I. Mossakowska, Polymorphs of p-nitrophenol as studied by variable-temperature X-ray diffraction and calorimetry: comparison with m-nitrophenol, Acta Crystallogr. B 62 (2006) 143-152.
[7] P. Naumov, K. Sakurai, M. Tanaka, H. Hara, Direct Observation of Aminyl Radical Intermediate during Single-Crystal to Single-Crystal Photoinduced Orton Rearrangement, The Journal of Physical Chemistry B 111 (2007) 10373-10378.
[8] K. Pilaniya, H. Chandrawanshi, U. Pilaniya, P. Manchandani, P. Jain, N. Singh, Recent trends in the impurity profile of pharmaceuticals, Journal of Advanced Pharmaceutical Technology & Research 1 (2010) 302-310.

[9] A. Llinàs, J.M. Goodman, Polymorph control: past, present and future, Drug Discovery Today 13 (2008) 198-210.
[10] R.R.E. Steendam, B. Harmsen, H. Meekes, W.J.P. van Enckevort, B. Kaptein, R.M. Kellogg, J. Raap, F.P.J.T. Rutjes, E. Vlieg, Controlling the effect of chiral impurities on Viedma ripening, Cryst. Growth Des. 13 (2013) 4776-4780.
[11] C. Schmidt, M.J. Jones, J. Ulrich, The Influence of Additives and Impurities on Crystallization, Crystallization, Wiley-VCH Verlag GmbH & Co. KGaA2013, pp. 105-127.
[12] K. Sangwal, Additives and Crystallization Processes: From Fundamentals to Applications, Additives and Crystallization Processes: From Fundamentals to Applications (2007).
[13] J. Peng, Y. Dong, L. Wang, L. Li, W. Li, H. Feng, Effect of Impurities on the Solubility, Metastable Zone Width, and Nucleation Kinetics of Borax Decahydrate, Industrial & Engineering Chemistry Research 53 (2014) 12170-12178.
[14] M. Jaoui, C. Achard, M. Rogalski, Solubility as a Function of Temperature of Selected Chlorophenols and Nitrophenols in Aqueous Solutions Containing Electrolytes or Surfactants, Journal of Chemical & Engineering Data 47 (2002) 297-303.
[15] C. Achard, M. Jaoui, M. Schwing, M. Rogalski, Aqueous Solubilities of Phenol Derivatives by Conductivity Measurements, Journal of Chemical & Engineering Data 41 (1996) 504-507.
[16] L.L. Carrick, Solubilities and Cooling Curves of Mononitrophenols, The Journal of Physical Chemistry 25 (1920) 628-659.
[17] B. de Souza, L. Keshavarz, G. Cogoni, P.J. Frawley, Pressurized-Synthetic Methodology for Solubility Determination at Elevated Temperatures with Application to Paracetamol in Pure Solvents, J. Chem. Eng. Data 62 (2017) 1689-1700.
[18] J.M. Prausnitz, R.N. Lichtenthaler, E.G. de Azevedo, Molecular thermodynamics of fluid-phase equilibria, Prentice-Hall1986.
[19] M. Kamberi, C.M. Riley, X. Ma, C.-W.C. Huang, A validated, sensitive HPLC method for the determination of trace impurities in acetaminophen drug substance, Journal of Pharmaceutical and Biomedical Analysis 34 (2004) 123-128.
[20] B.d. Souza, L. Keshavarz, R.R.E. Steendam, O.C. Dennehy, D. Lynch, S.G. Collins, H.A. Moynihan, A.R. Maguire, P.J. Frawley, Solubility Measurement and Thermodynamic Modelling of N-(4-methylphenyl-Z-3-chloro-2-(phenylthio)propenamide in Twelve Pure Solvents at Temperatures Ranging from (278.15 to 318.15) K, J. Chem. Eng. Data 63 (2018) 1419-1428.
[21] P. Coppens, G.M.J. Schmidt, The crystal structure of the [alpha]-modification of p-nitrophenol near 90degrees K, Acta Crystallographica 18 (1965) 62-67.
[22] R.A. Granberg, Å.C. Rasmuson, Solubility of Paracetamol in Pure Solvents, Journal of Chemical & Engineering Data 44 (1999) 1391-1395.
[23] B.E. Fisher, A.J. Tomson, J.P. Horwitz, 5-Aroyltetrazoles1, The Journal of Organic Chemistry 24 (1959) 1650-1654.
[24] N.N. Crounse, Isolation and Identification of a Metabolite of Chlorguanidine1, 2, The Journal of Organic Chemistry 16 (1951) 492-500.
[25] X.J. Wang, Q. Yang, F. Liu, Q.D. You, Microwave-Assisted Synthesis of Amide under Solvent-free Conditions, Synthetic Communications 38 (2008) 1028-1035.
[26] P.L. Southwick, H.L. Dimond, M.S. Moores, D.I. Sapper, A Cleavage of Certain α,β-Unsaturated Ketones by Alkaline Hydrogen Peroxide, J. Am. Chem. Soc. 78 (1956) 101-104.
[27] H. Eshghi, A. Hassankhani, E. Mosaddegh, Silica sulfuric acid as a reusable catalyst for the conversion of ketones into amides by a Schmidt reaction under solvent-free conditions, Journal of Chemical Research 2006 (2006) 218-219.
[28] D.E. Pearson, K.N. Carter, C.M. Greer, The Rearrangement of Hydrazones and Semicarbazones, J. Am. Chem. Soc. 75 (1953) 5905-5908.
[29] V.K. Redasani, V.S. Kumawat, R.P. Kabra, P. Kansagara, S. Surana, Applications of green chemistry in organic synthesis 2 (2010) 1856-1859.

[30] N.V. Sidgwick, H.E. Rubie, CIX.—The solubility and volatility of the chloro- and nitro-anilines and of their acetyl derivatives, Journal of the Chemical Society, Transactions 119 (1921) 1013-1024.
[31] F.L. Mota, A.P. Carneiro, A.J. Queimada, S.P. Pinho, E.A. Macedo, Temperature and solvent effects in the solubility of some pharmaceutical compounds: Measurements and modeling, European Journal of Pharmaceutical Sciences 37 (2009) 499-507.
[32] L. Keshavarz, R.R.E. Steendam, P.J. Frawley, Impact of Mother Liquor Recycle on the Impurity Buildup in Crystallization Processes, Organic Process Research & Development 22 (2018) 1541-1547.

Supporting Information

Table of contents

DSC Data

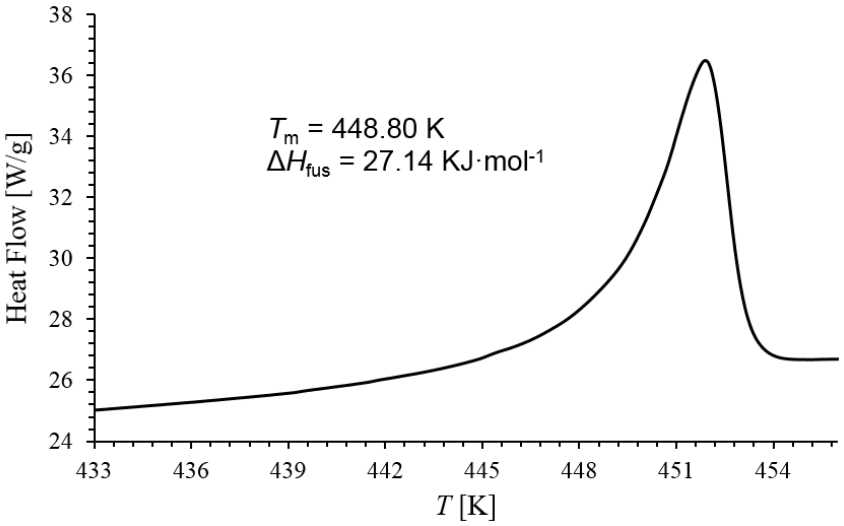

Fig. S1. DSC Thermogram of CA. The onset temperature of melting, obtained by taking the inflection point, was used as the melting temperature T_m.

HPLC Data

Table S1. HPLC Conditions for the Compounds Studied in this Work, Including Methanol / Phosphate Buffer Composition X of Mobile Phase, Wavelength λ of Detection, Retention Time t_R, and Concentration Range C_R.

chemical name	C_R [mg/L]	X [v/v%]	λ [nm]	t_R [min]
paracetamol (PA)	0-469	80/20	254	1.481
paracetamol (PA)	0-469	50/50	254	1.720
4'-chloroacetanilide (CA)	0-490	80/20	254	2.098
4-nitrophenol (NP)	0-130	50/50	310	4.576

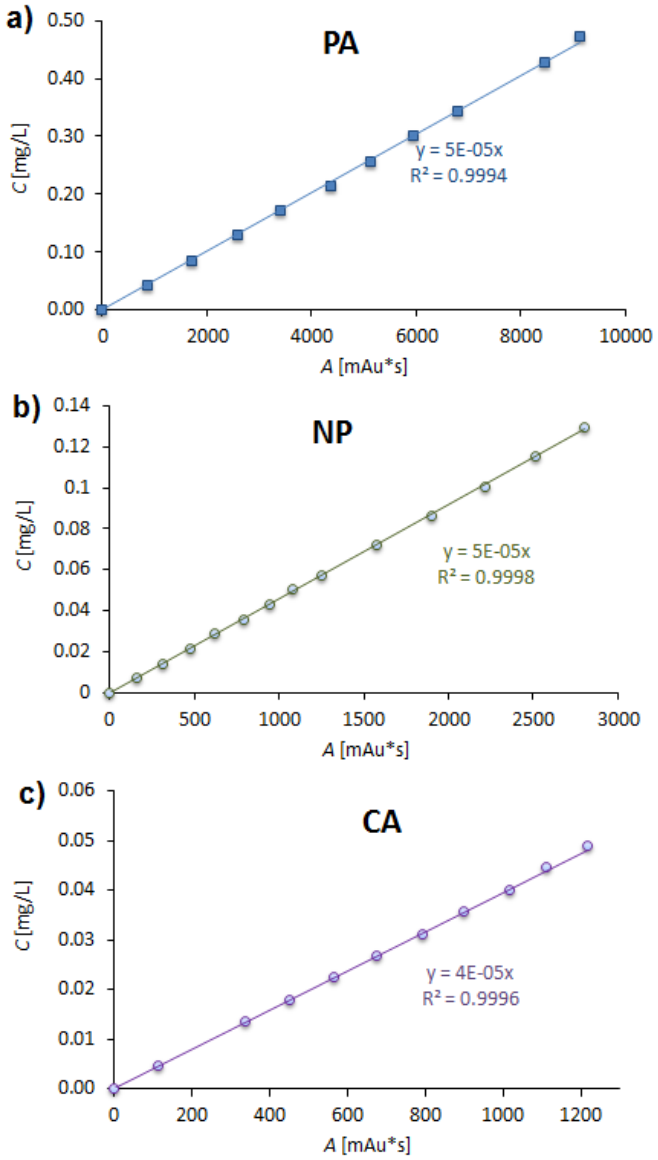

Fig. S2. HPLC calibration lines in which the concentration *C* is plotted versus the peak area *A* for a) PA, b) NP, c) CA. The equation for the linear calibration line and the quality R^2 of its fit is shown in each graph.

XRPD Data

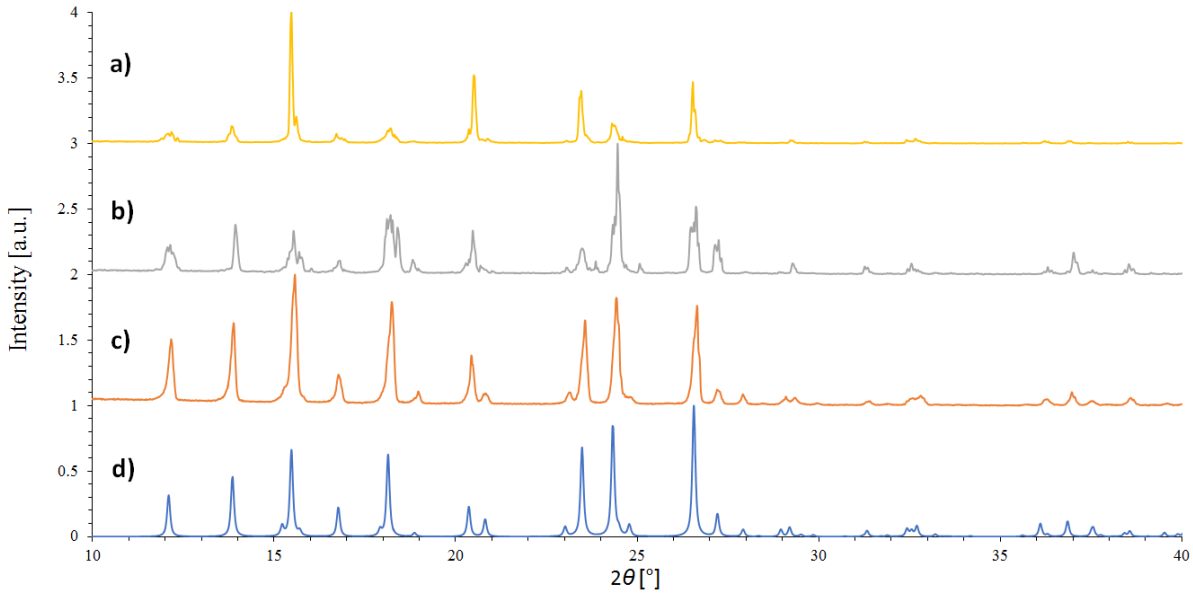

Fig. S3. XRPD Patterns of PA. a) After solubility measurements in the presence of 0.10 mole fraction of CA, b) after solubility measurements in the presence of 0.10 mole fraction of NP, c) raw material from Sigma Aldrich and d) Form I (CSD structure refcode HXACAN01).

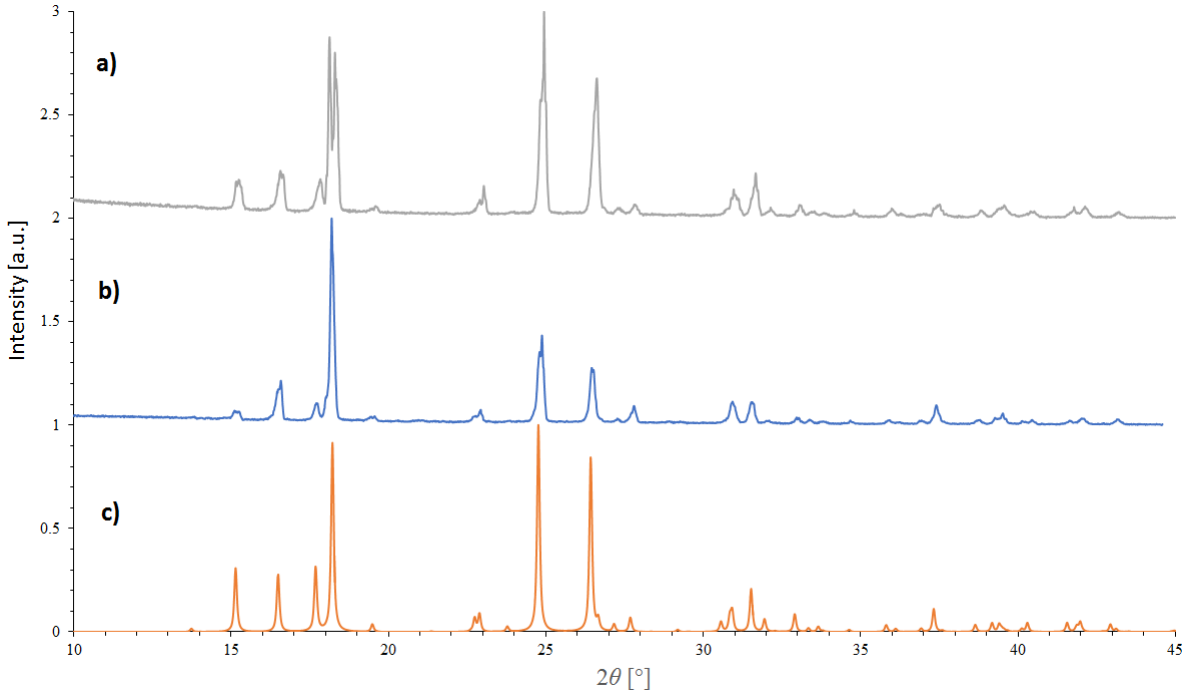

Fig. S4. XRPD Patterns of CA. a) Representative sample after solubility measurements, b) raw material from Sigma Aldrich and c) CSD structure refcode CLACTN.

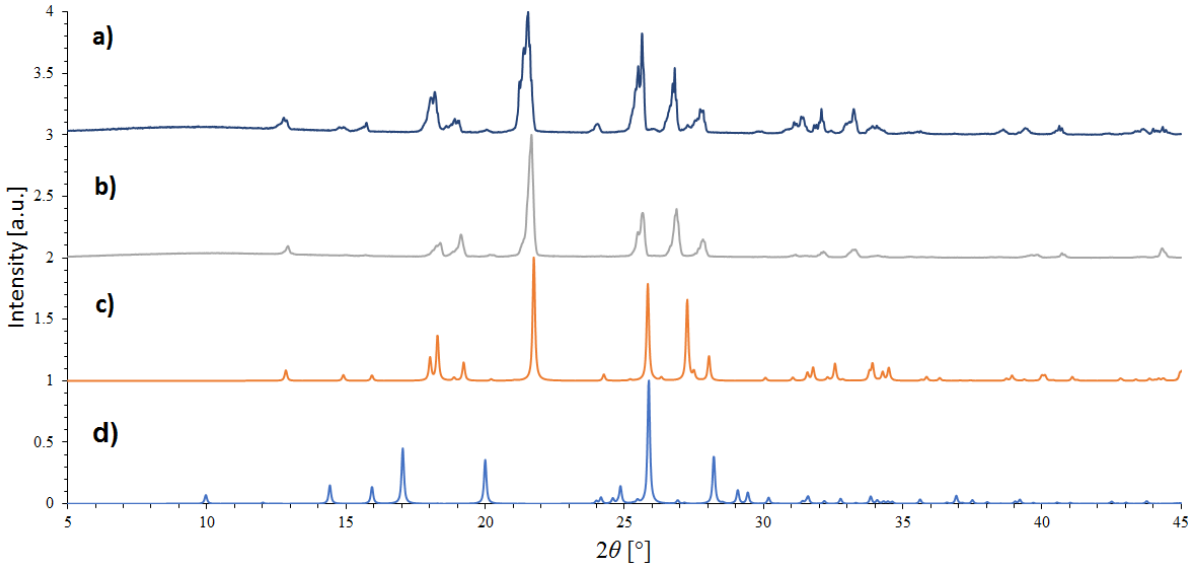

Fig. S5. XRPD Patterns of NP. a) Representative sample after solubility measurements, b) raw material from Alfa Aesar, c) α-NP (CSD structure refcode NITPOL01) and d) β-NP (CSD structure refcode NITPOL).

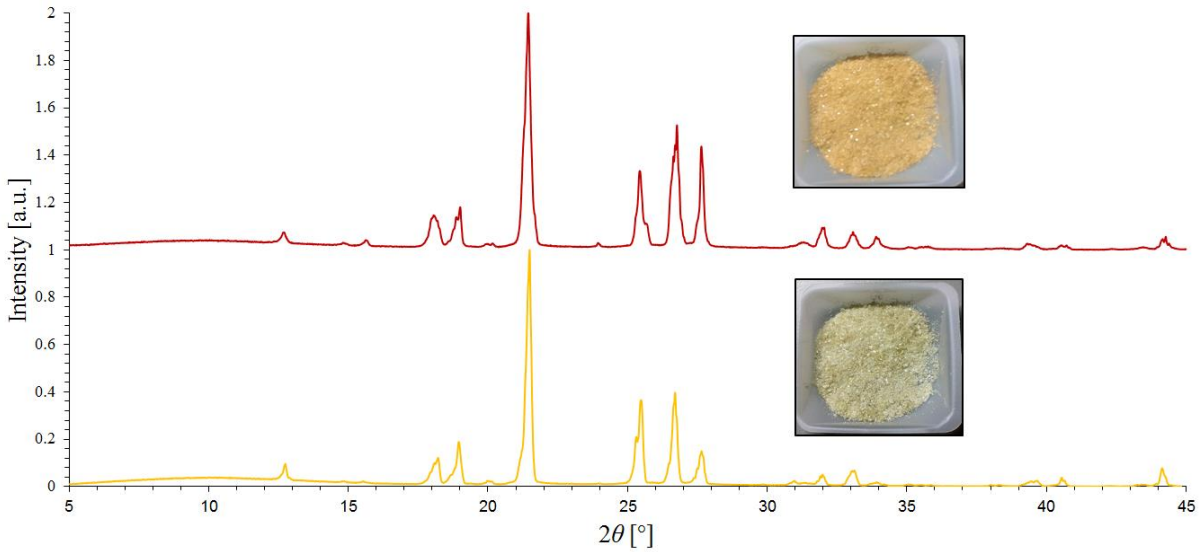

Fig. S6. XRPD Patterns of α-NP crystals before (bottom) and after (top) being exposed for 48 hours to visible light. The insets show photographs of the crystals.

Solubility Data Impurities

Table S2. Experimental Mass-Fraction Solubility *C*, Mole Fraction Solubility x^{exp} and Calculated Mole Fraction Solubility Data of CA in Four Different Alcohols at Saturation Temperature *T* and Pressure *p* = 0.1 MPa.[a]

T [*K*]	*C* [g/kg]	x^{exp}	x^{apel}	x^{Marg}	x^{VL}	x^{W}	x^{NRTL}
			ethanol				
278.15	31.286	0.0087	0.0085	0.0064	0.0065	0.0073	0.0085
283.15	35.090	0.0098	0.0099	0.0079	0.0080	0.0087	0.0098
288.15	40.611	0.0114	0.0114	0.0098	0.0098	0.0105	0.0114
293.15	45.181	0.0127	0.0131	0.0120	0.0119	0.0124	0.0131
298.15	53.320	0.0151	0.0151	0.0147	0.0144	0.0147	0.0150
303.15	60.802	0.0173	0.0173	0.0178	0.0172	0.0173	0.0173
308.15	69.872	0.0200	0.0198	0.0214	0.0205	0.0202	0.0198
313.15	78.630	0.0227	0.0226	0.0256	0.0243	0.0235	0.0226
318.15	88.453	0.0257	0.0258	0.0305	0.0286	0.0273	0.0258
323.15	100.02	0.0293	0.0293	0.0362	0.0335	0.0315	0.0294
328.15	112.70	0.0333	0.0333	0.0427	0.0391	0.0362	0.0334
			2-propanol				
278.15	25.394	0.0091	0.0093	0.0066	0.0069	0.0073	0.0092
283.15	28.862	0.0104	0.0104	0.0082	0.0084	0.0088	0.0104
288.15	33.542	0.0121	0.0118	0.0101	0.0103	0.0106	0.0119
293.15	36.948	0.0134	0.0134	0.0124	0.0125	0.0126	0.0134
298.15	41.179	0.0150	0.0153	0.0151	0.0151	0.0150	0.0152
303.15	47.568	0.0174	0.0174	0.0183	0.0181	0.0177	0.0174
308.15	53.885	0.0198	0.0199	0.0220	0.0215	0.0208	0.0198
313.15	62.465	0.0231	0.0228	0.0263	0.0255	0.0243	0.0228
318.15	70.797	0.0263	0.0261	0.0314	0.0300	0.0283	0.0261
323.15	79.325	0.0296	0.0301	0.0371	0.0352	0.0327	0.0299
328.15	92.231	0.0348	0.0346	0.0438	0.0410	0.0378	0.0347
			1-butanol				
278.15	24.777	0.0110	0.0108	0.0079	0.0081	0.0086	0.0109
283.15	27.409	0.0122	0.0123	0.0098	0.0100	0.0104	0.0124
288.15	32.125	0.0143	0.0140	0.0121	0.0122	0.0125	0.0141
293.15	35.739	0.0159	0.0160	0.0147	0.0148	0.0149	0.0160
298.15	39.858	0.0178	0.0182	0.0179	0.0178	0.0177	0.0181
303.15	46.137	0.0207	0.0208	0.0216	0.0213	0.0209	0.0207
308.15	52.414	0.0236	0.0237	0.0259	0.0254	0.0246	0.0236
313.15	60.165	0.0272	0.0270	0.0309	0.0301	0.0287	0.0270
318.15	68.769	0.0313	0.0308	0.0367	0.0354	0.0334	0.0309
323.15	76.476	0.0349	0.0351	0.0433	0.0415	0.0386	0.0352
328.15	86.995	0.0400	0.0400	0.0510	0.0484	0.0445	0.0403
			1-pentanol				
278.15	23.267	0.0122	0.0121	0.0091	0.0092	0.0098	0.0123
283.15	26.636	0.0140	0.0139	0.0112	0.0113	0.0118	0.0140
288.15	30.405	0.0160	0.0159	0.0138	0.0138	0.0142	0.0159
293.15	34.112	0.0180	0.0182	0.0168	0.0167	0.0170	0.0181
298.15	38.711	0.0205	0.0207	0.0204	0.0202	0.0202	0.0206
303.15	43.265	0.0230	0.0237	0.0245	0.0242	0.0238	0.0234
308.15	50.696	0.0270	0.0270	0.0293	0.0288	0.0279	0.0269
313.15	58.409	0.0312	0.0309	0.0349	0.0341	0.0326	0.0308
318.15	66.130	0.0355	0.0352	0.0413	0.0402	0.0380	0.0352
323.15	74.642	0.0402	0.0401	0.0487	0.0471	0.0439	0.0402
328.15	83.528	0.0452	0.0456	0.0571	0.0549	0.0506	0.0459

[a] Standard uncertainty for temperature is $u(T)$ = 0.2 K. Type A relative standard uncertainties for pressure and mass-fraction solubility and mole fraction solubility are $u_r(p)$=0.05, $u_r(C)$=0.0185 and $u_r(x_2)$ =0.0156, respectively.

Table S3. Experimental Mass-Fraction Solubility *C* and Mole Fraction Solubility x^{exp} and Calculated Mole Fraction Solubility Data of α-NP in Four Different Alcohols at Temperature *T* and Pressure *p*=0.1 MPa.[a]

T [*K*]	*C* [g/kg]	x^{exp}	x^{apel}	x^{Marg}	x^{VL}	x^{W}	x^{NRTL}
			ethanol				
278.15	575.56	0.3099	0.3053	0.2765	0.3313	0.3048	0.3118
283.15	593.59	0.3260	0.3235	0.3009	0.3257	0.3227	0.3252
288.15	604.94	0.3365	0.3422	0.3270	0.3409	0.3421	0.3410
293.15	627.32	0.3579	0.3614	0.3533	0.3519	0.3604	0.3570
298.15	645.81	0.3765	0.3810	0.3810	0.3721	0.3797	0.3751
303.15	670.25	0.4023	0.4010	0.4092	0.3941	0.3987	0.3947
308.15	686.05	0.4198	0.4214	0.4395	0.4217	0.4197	0.4167
313.15	709.44	0.4471	0.4423	0.4700	0.4499	0.4401	0.4405
318.15	729.28	0.4715	0.4635	0.5020	0.4808	0.4619	0.4665
323.15	740.59	0.4860	0.4851	0.5363	0.5144	0.4861	0.4942
328.15	750.96	0.4996	0.5070	0.5719	0.5496	0.5114	0.5235
			2-propanol				
278.15	532.26	0.3296	0.3255	0.2948	0.3355	0.3161	0.3359
283.15	552.14	0.3475	0.3448	0.3191	0.3393	0.3350	0.3469
288.15	561.22	0.3559	0.3640	0.3461	0.3604	0.3565	0.3619
293.15	582.47	0.3760	0.3831	0.3723	0.3728	0.3763	0.3760
298.15	609.68	0.4029	0.4021	0.3985	0.3870	0.3954	0.3912
303.15	628.75	0.4225	0.4207	0.4271	0.4098	0.4167	0.4098
308.15	650.18	0.4454	0.4391	0.4562	0.4343	0.4380	0.4302
313.15	660.48	0.4567	0.4572	0.4886	0.4646	0.4624	0.4533
318.15	679.05	0.4776	0.4749	0.5204	0.4939	0.4858	0.4778
323.15	688.55	0.4885	0.4921	0.5552	0.5273	0.5119	0.5043
328.15	705.52	0.5086	0.5090	0.5895	0.5603	0.5372	0.5327
			1-butanol				
278.15	422.18	0.2802	0.2838	0.2471	0.2839	0.2670	0.2902
283.15	452.04	0.3053	0.2986	0.2707	0.2829	0.2849	0.3001
288.15	465.77	0.3172	0.3142	0.2957	0.3045	0.3050	0.3132
293.15	473.92	0.3243	0.3306	0.3220	0.3297	0.3264	0.3277
298.15	497.71	0.3455	0.3479	0.3497	0.3543	0.3471	0.3436
303.15	518.12	0.3642	0.3661	0.3787	0.3819	0.3688	0.3616
308.15	551.25	0.3956	0.3853	0.4090	0.4108	0.3901	0.3826
313.15	562.38	0.4064	0.4054	0.4408	0.4422	0.4144	0.4039
318.15	581.11	0.4250	0.4265	0.4738	0.4749	0.4388	0.4279
323.15	602.15	0.4464	0.4487	0.5082	0.5089	0.4640	0.4544
328.15	627.70	0.4732	0.4720	0.5439	0.5443	0.4897	0.4844
			1-pentanol				
278.15	376.94	0.2771	0.2772	0.2374	0.2343	0.2530	0.2827
283.15	390.26	0.2886	0.2913	0.2606	0.2568	0.2725	0.2929
288.15	415.67	0.3107	0.3061	0.2855	0.2806	0.2919	0.3044
293.15	424.28	0.3183	0.3217	0.3113	0.3056	0.3135	0.3178
298.15	446.59	0.3383	0.3381	0.3389	0.3319	0.3347	0.3331
303.15	471.94	0.3616	0.3553	0.3680	0.3595	0.3566	0.3507
308.15	483.44	0.3723	0.3734	0.3981	0.3883	0.3805	0.3691
313.15	503.71	0.3914	0.3924	0.4298	0.4185	0.4045	0.3902
318.15	517.84	0.4050	0.4123	0.4628	0.4499	0.4299	0.4124
323.15	550.35	0.4368	0.4332	0.4977	0.4826	0.4549	0.4405
328.15	569.24	0.4557	0.4551	0.5336	0.5166	0.4820	0.4682

[a] Standard uncertainty for temperature is $u(T)$ = 0.2 K. Type A relative standard uncertainties for pressure, mass-fraction solubility and mole solubility are $u_r(p)$=0.05, $u_r(C)$=0.0051 and $u_r(x_2)$=0.0033, respectively.

Modelling Data

Table S4. Apelblat Parameters and Mean Square Error (MSE) for Each Solubility System.

solute	solvent	a_A	b_A	c_A	MSE
CA	ethanol	-5.6796×10^{1}	2.5280×10^{2}	9.0833	2.0213×10^{-5}
CA	2-propanol	-1.5919×10^{2}	4.9285×10^{3}	2.4305×10^{1}	1.8292×10^{-6}
CA	1-butanol	-1.0570×10^{2}	2.5457×10^{3}	1.6351×10^{1}	4.9189×10^{-6}
CA	1-pentanol	-9.0249×10^{1}	1.8314×10^{3}	1.4081×10^{1}	2.8515×10^{-5}
α-NP	ethanol	-1.4472	-7.6476×10^{2}	5.3483×10^{-1}	4.9799×10^{-5}
α-NP	2-propanol	3.0708×10^{1}	-2.1149×10^{3}	-4.3046	1.2214×10^{-4}
α-NP	1-butanol	-3.8500×10^{1}	8.9547×10^{2}	6.0448	4.2390×10^{-4}
α-NP	1-pentanol	-3.7694×10^{1}	8.7787×10^{2}	5.9087	1.4614×10^{-5}

Table S5. Estimated Binary Coefficients for CA in Four Different Alcohols Using Margules, van Laar, Wilson and NRTL Models.

	Margules	van Laar		Wilson		NRTL		
solvent	A	A_{VL}	B_{VL}	λ_{12}	λ_{21}	g_{12}	g_{21}	α
ethanol	1.4002×10^{3}	6.5680×10^{7}	5.6820×10^{-1}	1.4380×10^{6}	-2.9548×10^{3}	4.9852×10^{5}	-4.8863×10^{5}	8.8042×10^{-5}
2-propanol	1.3257×10^{3}	5.0124×10^{7}	5.1912×10^{-1}	4.4706×10^{6}	-2.3350×10^{3}	3.2455×10^{4}	-2.0450×10^{4}	4.9412×10^{-2}
1-butanol	8.9549×10^{2}	9.7574×10^{6}	3.5331×10^{-1}	8.0444×10^{5}	-2.3132×10^{3}	3.4470×10^{4}	-2.3530×10^{4}	3.6562×10^{-2}
1-pentanol	5.6534×10^{2}	1.2045×10^{6}	2.2596×10^{-1}	6.7408×10^{5}	-2.2213×10^{3}	3.3217×10^{4}	-2.3112×10^{4}	3.6149×10^{-2}

Table S6. Estimated Binary Coefficients for α-NP in Four Different Alcohols Using Margules, van Laar, Wilson and NRTL Models.

	Margules	van Laar		Wilson		NRTL		
solvent	A	A_{VL}	B_{VL}	λ_{12}	λ_{21}	g_{12}	g_{21}	α
ethanol	-5.6016×10^{2}	1.7100×10^{-2}	-5.4401×10^{-2}	7.3124×10^{5}	-4.2806×10^{3}	1.4264×10^{6}	-1.4173×10^{6}	1.1789×10^{-5}
2-propanol	-9.2241×10^{2}	8.1376×10^{-2}	-3.3896×10^{-1}	4.2548×10^{5}	-3.7926×10^{3}	3.3489×10^{6}	-3.3385×10^{6}	2.4828×10^{-6}
1-butanol	-1.1749×10^{1}	-2.4050×10^{-3}	2.5809×10^{-3}	4.0882×10^{5}	-2.8182×10^{3}	3.3495×10^{6}	-3.3379×10^{6}	2.5442×10^{-6}
1-pentanol	1.4881×10^{2}	-1.0966×10^{-2}	1.0170×10^{-2}	3.0981×10^{5}	-2.2612×10^{3}	1.9278×10^{6}	-1.9140×10^{6}	9.1052×10^{-6}

Table S7. Mean Squared Errors (MSE) of the Fitted Thermodynamic Models for Each Solvent and Solute.

solute	solvent	Margules	van Laar	Wilson	NRTL	MSE_{max}/MSE_{min}
CA	ethanol	3.7806×10^{-2}	2.5415×10^{-2}	6.3107×10^{-3}	1.0449×10^{-4}	3.6182×10^{2}
CA	2-propanol	4.8002×10^{-2}	4.3607×10^{-2}	1.6110×10^{-2}	2.1622×10^{-4}	2.2200×10^{2}
CA	1-butanol	4.0655×10^{-2}	3.4473×10^{-2}	1.2943×10^{-2}	1.7189×10^{-4}	2.3652×10^{2}
CA	1-pentanol	3.5145×10^{-2}	3.3224×10^{-2}	1.2726×10^{-2}	1.7624×10^{-4}	1.9942×10^{2}
α-NP	ethanol	7.1766×10^{-3}	1.3303×10^{-3}	2.9108×10^{-4}	4.1233×10^{-4}	2.4655×10^{1}
α-NP	2-propanol	8.2794×10^{-3}	2.5874×10^{-3}	1.3751×10^{-3}	9.7714×10^{-4}	8.4731
α-NP	1-butanol	1.1196×10^{-2}	9.5545×10^{-3}	1.6522×10^{-3}	5.9021×10^{-4}	1.8969×10^{1}
α-NP	1-pentanol	1.3732×10^{-2}	1.2356×10^{-2}	2.7941×10^{-3}	5.2836×10^{-4}	2.5990×10^{1}

References Supporting Information

1. B. de Souza, L. Keshavarz, G. Cogoni and P. J. Frawley, *Journal of Chemical & Engineering Data*, 2017, **62**, 1689-1700.